Hybrid-PIC Modeling of the Transport of Atomic Boron in a Hall Thruster

IEPC-2015-252／ISTS-2015-b-252

Presented at Joint Conference of 30th International Symposium on Space Technology and Science, 34th International Electric Propulsion Conference and 6th Nano-satellite Symposium
Hyogo-Kobe, Japan
July 4–10, 2015

Brandon D. Smith* and Iain D. Boyd†
University of Michigan, Ann Arbor, Michigan, 48109, USA

and

Hani Kamhawi‡
NASA Glenn Research Center, Cleveland, Ohio, 44135, USA

Abstract: Computational analysis of the transport of boron eroded from the walls of a Hall thruster is performed by implementing sputter yields of hexagonal boron nitride and velocity distribution functions of boron within the hybrid-PIC model HPHall. The model is applied to simulate NASA's HiVHAc Hall thruster at a discharge voltage of 500 V and discharge powers of 1–3 kW. The number densities of ground- and ^{4}P-state boron are computed. The density of ground-state boron is shown to be a factor of about 30 less than the plasma density. The density of the excited state is shown to be about three orders of magnitude less than that of the ground state, indicating that electron impact excitation does not significantly affect the density of ground-state boron in the discharge channel or near-field plume of a Hall thruster. Comparing the rates of excitation and ionization suggests that ionization has a greater influence on the density of ground-state boron, but is still negligible. The ground-state boron density is then integrated and compared to cavity ring-down spectroscopy (CRDS) measurements for each operating point. The simulation results show good agreement with the measurements for all operating points and provide evidence in support of CRDS as a tool for measuring Hall thruster erosion *in situ*.

Nomenclature

B	= magnetic field magnitude
E	= kinetic energy of incident ion
E_b	= surface binding energy of boron to h-BN
E_{th}	= threshold energy for sputtering
I_d	= thruster discharge current
L	= thruster discharge channel length
N_B	= number of boron macroparticles generated per ion impact
T_e	= electron temperature
T_p, T_t	= boron temperature along the forward and transverse sputtering directions
V_d	= thruster discharge voltage

*Ph.D. candidate, Department of Aerospace Engineering, bradenis@umich.edu
†James E. Knott Professor, Department of Aerospace Engineering, iainboyd@umich.edu
‡Research Engineer, In-Space Propulsion Systems, hani.kamhawi-1@nasa.gov.

W = macroparticle numerical weight
Y = integrated sputter yield
Y_0 = sputter yield at normal ion incidence
e = elementary charge
k_B = Boltzmann constant
m_B = molecular mass of boron
n_B = boron number density
n_e = electron number density
n_{PI} = path-integrated boron number density
$\hat{\boldsymbol{n}}$ = wall normal vector
$\hat{\boldsymbol{p}}, \hat{\boldsymbol{t}}$ = unit vectors defining forward and transverse sputtering directions
$\boldsymbol{v}$ = velocity vector
v_b = effective binding velocity
r_{inner} = radius of inner channel wall
r_{outer} = radius of outer channel wall
z, r = axial and radial coordinates
Ω_e = electron Hall parameter
λ = magnetic stream function
$\mu_{e,\perp}$ = electron mobility across magnetic field lines
ν_e = total effective collision frequency for electrons
ν_B = anomalous Bohm collision frequency
ν_{ei}, ν_{en} = electron-ion and electron neutral collision frequency
ν_w = electron-wall collision frequency
θ = ion incidence angle
ϕ = plasma potential
ϕ^* = thermalized plasma potential

I. Introduction

Historically, the life-limiting mechanism of Hall thrusters has been the erosion of the discharge channel walls via ion bombardment. During thruster operation, energetic ions from the plasma discharge strike the walls, causing atomic sputtering. These sputtering events accumulate over time to produce macroscopic erosion. The channel walls, typically made of hexagonal boron nitride (h-BN) or a BN-based ceramic, shield the magnetic coils and pole pieces from the plasma. Once the erosion process exposes the coils and pole pieces to the plasma, the magnetic topography in the discharge channel begins to change, ultimately resulting in thruster failure. This erosion process also produces free-moving condensible species, namely atomic boron, that may deposit on thruster surfaces, effectively reducing the observed erosion rate, or on mission-critical spacecraft surfaces such as solar panels or optical instruments. Hence, understanding this erosion process is of great importance to future missions utilizing Hall thrusters.

Experimental characterization of Hall thruster operational lifetime is typically performed by operating the thruster under high-vacuum conditions until thruster failure. This process takes at least several thousand hours, making it both time-consuming and expensive. This has motivated several efforts to perform quickly characterize thruster lifetime via numerical modeling.[1–4] However, none of these efforts have attempted to capture the behavior of the erosion products. Modern diagnostic tools such as cavity ring-down spectroscopy (CRDS)[5] have enabled *in situ* measurement of the density of erosion products, providing a novel means by which to validate Hall thruster erosion models. This work applies a hybrid fluid–particle-in-cell (hybrid-PIC) model to simulate Hall thruster channel wall erosion. The h-BN sputter yields are computed using a high-speed, physics-based molecular dynamics (MD) model of h-BN sputtering by energetic xenon ions.[6] The computed sputter yields and the 3D velocity distribution function (VDF) of atomic boron are included in the hybrid-PIC model. The macroscopic erosion rate is calculated based on the properties of ions striking the

walls and on the computed sputter yields. Boron particles are then generated within the model according to the VDFs from the MD model, and the boron number density is recorded. These results are then processed and compared to measurements of path-integrated boron density obtained using CRDS.

The remainder of this paper is organized as follows: Section II discusses the details of the hybrid-PIC model and the implementation of the sputter yield results. Section III presents the simulation results and compares them to the experimental measurements. Finally, Section IV summarizes the findings and outlines paths for future work.

II. Model overview

A. Hybrid-PIC model

The numerical model used in this work is HPHall-3.[7] HPHall simulates a Hall thruster discharge plasma using an axisymmetric hybrid-PIC method in which the ions and neutrals are modeled using PIC and the electrons are treated as a quasi-1D fluid. The plasma is assumed to be quasineutral throughout the simulation domain, and the local plasma density is computed from the PIC submodel. The plasma potential is computed from the well-known thermalized potential approximation:

$$\phi^*(\lambda) = \phi - \frac{k_B T_e(\lambda)}{e} \ln\left(\frac{n_e}{n_{e,0}}\right) \tag{1}$$

where ϕ^* and T_e are constant along magnetic field lines. The thermalized potential ϕ^* is computed via momentum conservation across magnetic field lines, and the electron temperature T_e is computed from energy conservation. Induced magnetic fields are assumed to be much smaller in magnitude than the applied magnetic field, which is supplied as an input to the model.

A principal characteristic of HPHall is its treatment of the electron mobility across magnetic field lines. In general, the cross-field mobility can be written as

$$\mu_{e,\perp} = \frac{e}{m_e \nu_e} \frac{1}{1+\Omega_e^2} \approx \frac{m_e \nu_e}{eB^2} \tag{2}$$

for large values of Ω_e. Assuming the effects of electron-electron scattering collisions are negligible, the effective collision frequency ν_e can be written as

$$\nu_e = \nu_{ei} + \nu_{en} + \nu_w + \nu_B, \tag{3}$$

where ν_B is the anomalous Bohm collision frequency, given by

$$\nu_B = \alpha \frac{1}{16} \frac{eB}{m_e}. \tag{4}$$

The parameter α is an empirical coefficient that sets the degree to which the Bohm diffusion term affects the electron motion. This value is defined independently in three regions of the thruster:[8] the near-anode or discharge channel region, denoted by the letter c; the exit region, denoted by the letter e; and the plume region, denoted by the letter p. At the boundaries between regions is a buffer zone in which the value of α is interpolated linearly between the values in the neighboring Bohm regions. The exact location of these buffer zones is left to the user, as there is no *a priori* means to determine their optimal location. In this work, the α values and the location of each buffer zone is determined by first setting values of $\alpha_c = 0.2$, $\alpha_e = 0.02$, and $\alpha_p = 10.0$, and then adjusting the location of each buffer zone to roughly match the calculated discharge current to experimental measurements. Then, the values of α_c and α_e are adjusted to better match the measured discharge current. This process is repeated until the calculated discharge current matches the measured current to within a few percent.

B. Sputter yield calculation

To compute the sputter yield—and thus the erosion rate—when an ion strikes the discharge channel wall, one must know the incidence angle and kinetic energy of the impacting ion. The incidence angle is calculated

based on the ion's velocity vector at the sheath edge, the floating sheath potential, and the wall normal. If $\boldsymbol{v}_1$ is the velocity vector at the sheath edge and $\boldsymbol{v}_2$ is the velocity vector at the wall:

$$\begin{aligned}\boldsymbol{v}_1 &= v_z\hat{\boldsymbol{z}} + v_r\hat{\boldsymbol{r}} + v_\theta\hat{\boldsymbol{\theta}}\\ \boldsymbol{v}_2 &= (v_z + \Delta v_z)\,\hat{\boldsymbol{z}} + (v_r + \Delta v_r)\,\hat{\boldsymbol{r}} + v_\theta\hat{\boldsymbol{\theta}}\end{aligned}$$

where the geometry is assumed to be axisymmetric and the electric field in the sheath is assumed to act normal to the wall. We need to solve for both Δv_z and Δv_r in order to obtain the ion incidence angle. From energy conservation:

$$|\boldsymbol{v}_2|^2 - |\boldsymbol{v}_1|^2 = \frac{2q\phi_s}{m} \tag{5}$$

where the sheath potential ϕ_s is known. This also gives the kinetic energy at the wall directly. One can define a spatial coordinate n that points in the direction of the inward-facing wall normal vector $\hat{\boldsymbol{n}}$. Momentum conservation then gives

$$\begin{aligned}-q\nabla\phi &= m\frac{d\boldsymbol{v}}{dt},\\ -q\frac{d\phi}{dn}\hat{\boldsymbol{n}} &= m\frac{d\boldsymbol{v}}{dt},\\ -q\frac{d\phi}{dn}\left(n_z\hat{\boldsymbol{z}} + n_r\hat{\boldsymbol{r}}\right) &= m\frac{d}{dt}\left(v_z\hat{\boldsymbol{z}} + v_r\hat{\boldsymbol{r}} + v_\theta\hat{\boldsymbol{\theta}}\right).\end{aligned} \tag{6}$$

Manipulating the $\hat{\boldsymbol{z}}$ and $\hat{\boldsymbol{r}}$ components of Eq. 6 and combining them gives

$$\begin{aligned}n_r\frac{dv_z}{dt} &= n_z\frac{dv_r}{dt},\\ n_r\Delta v_z &= n_z\Delta v_r.\end{aligned} \tag{7}$$

Substituting from Eq. 7 into Eq. 5 then gives a quadratic equation for either Δv_z or Δv_r. Solving for Δv_z gives:

$$\Delta v_z = \frac{-\left(v_z + \frac{v_r n_r}{n_z}\right) \pm \sqrt{\left(v_z + \frac{v_r n_r}{n_z}\right)^2 + \left(1 + \frac{n_r^2}{n_z^2}\right)\left(\frac{2q\phi_s}{m}\right)}}{1 + \frac{n_r^2}{n_z^2}}. \tag{8}$$

The term inside the square root is always positive. For $v_z < 0$ we take the negative root. For $v_z > 0$ we take the positive root. Δv_r is then found by substituting Δv_z into Eq. 7. In the limiting case of $n_z = 0$:

$$\begin{aligned}\Delta v_z &= 0,\\ \Delta v_r &= -v_r \pm \sqrt{v_r^2 + \frac{2q\phi_s}{m}}.\end{aligned} \tag{9}$$

Now $\boldsymbol{v}_2$ is known, so the incidence angle relative to the wall normal is simply

$$\theta = \cos^{-1}\left(\frac{\boldsymbol{v}_2 \cdot \hat{\boldsymbol{n}}}{|\boldsymbol{v}_2|}\right). \tag{10}$$

With the kinetic energy and incidence angle of the ion known, one can compute the sputter yield. We start with a Bohdansky fit to the sputter yields at normal ion incidence:[6,9]

$$Y_0(E) = \gamma\left[1 - \left(\frac{E_{th}}{E}\right)^{2/3}\right]\left(1 - \frac{E_{th}}{E}\right)^2. \tag{11}$$

The parameter γ is the sputter yield in the limit $E \to \infty$ and E_{th} is the threshold energy for sputtering. Two sets of parameters are found when fitting the Bohdansky function to the calculated sputter yields, depending on the initial parameters used. The two sets of parameters are shown in Table 2. Note that these are total sputter

Table 2: Bohdansky parameter values for normal ion incidence. The error is computed based on 95% confidence bounds from the least-squares fitting process.

	γ, atoms/ion	E_{th}, eV
Fit a	0.4 ± 0.3	36 ± 3
Fit b	1.3 ± 1.1	48 ± 9

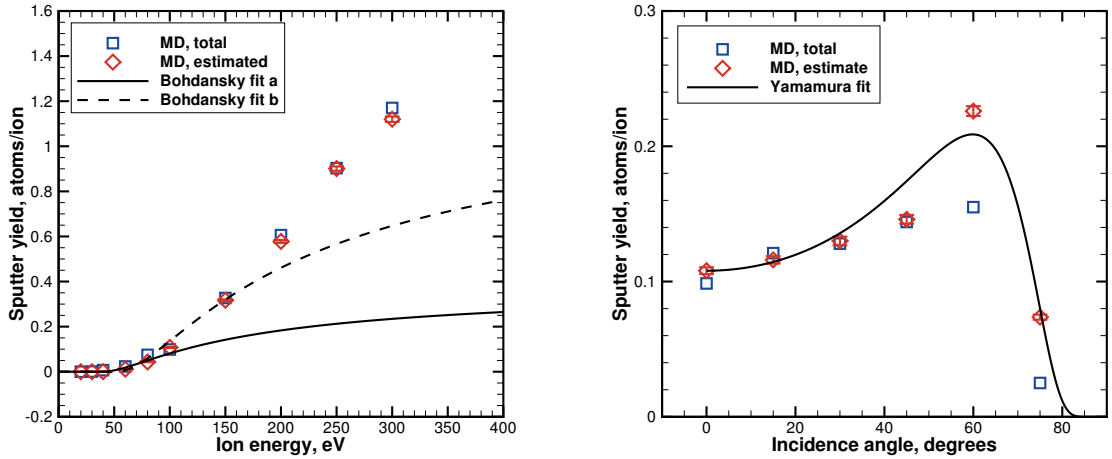

(a) (b)

Figure 1: *h*-BN sputter yields: (a) As a function of ion energy at normal incidence and (b) as a function of incidence angle at 100 eV energy. Calculation details are contained in Ref. 6.

yields, which include both nitrogen and boron. Experimental[10] and numerical[6,11] efforts have found evidence that *h*-BN tends to sputter in the form of B_x and N_y $(x, y \geq 1)$, with molecules of B and N appearing rarely. In particular, nitrogen tends to sputter as N_2 and boron tends to sputter as B. Thus, the yield of atomic boron is simply $1/2$ the total yield, and the values of γ used in HPHall are $1/2$ those given in Table 2.

The yield at normal incidence can be used as an input to a Yamamura function:[12]

$$Y_Y(\theta) = Y_0(E)\cos^A(\theta)\exp\left[-B\left(\frac{1}{\cos(\theta)}-1\right)\right]\left[\frac{1-\sqrt{\frac{E_{th,Y}}{E}}\cos(\theta)}{1-\sqrt{\frac{E_{th,Y}}{E}}}\right] \tag{12}$$

where A, B, and $E_{th,Y}$ are treated as free fit parameters, although $E_{th,Y}$ is typically interpreted as the threshold energy for sputtering. This curve is fit in a least-squares sense to the data from the MD model. Table 3 shows the computed fit parameters for ion energies of 100 eV and 250 eV. Note that $E_{th,Y}$ is found to be zero for both ion energies. For this reason, $E_{th,Y}$ is only treated as a free fit parameter in this work, whereas E_{th} in Eq. 11 is interpreted as the threshold energy for sputtering. For the purposes of this work, the Yamamura parameters for 100 eV are used regardless of ion energy. Figure 1 shows the sputter yields used along with the corresponding Bohdansky and Yamamura curve fits.

Table 3: Yamamura fit parameters for ion energies of 100 eV and 250 eV.

Ion energy	A	B	$E_{th,Y}$, eV
100 eV	-3.5	1.7	0.0
250 eV	-2.4	0.92	0.0

C. Atomic boron modeling

One of the principal goals of this work is to predict the transport of atomic boron through a Hall thruster. Knowing the boron density throughout the simulation domain will allow direct comparison of the simulation results to *in situ* erosion diagnostics such as cavity ring-down spectroscopy.[5] To accurately calculate the boron density, one must capture the behavior of the boron atoms as they leave the walls and are transported through the thruster.

Each time an ion macroparticle strikes the discharge channel wall, the sputter yield is computed according to Eqs. 11 and 12. Boron macroparticles must then be generated such that the number of real boron atoms introduced matches the calculated sputter yield. If the ion macroparticle has numerical weight W_{ion} and N_B boron macroparticles are produced each time an ion strikes the wall, then the numerical weight of each boron macroparticle is given by

$$W_B = \frac{W_{ion} Y}{N_B}. \tag{13}$$

For cases when the calculated yield Y is very small, W_B may be less than 1. This is nonphysical, so a minimum allowable sputter yield is set such that a minimum macroparticle weight of 100 is maintained. When the calculated yield is less than the minimum, a random number between 0 and 1 is generated and compared to the value

$$\frac{Y_{min} - Y_{calc}}{Y_{min}}.$$

If the random number is less than this value, boron macroparticles are generated according to Eq. 13 with $Y = Y_{min}$. Otherwise, no boron macroparticles are generated.

The directions of forward and transverse sputtering in cylindrical polar coordinates must be known in order to assign the correct velocity vector to the ejected boron atoms. These are computed from the known surface normal vector and the incident ion's velocity vector, $\boldsymbol{v}_2$. The unit vector $\hat{\boldsymbol{p}}$ defining the forward sputtering direction is computed as

$$\hat{\boldsymbol{p}} = \frac{\sqrt{\left(v_z + \Delta v_z\right)^2 \left(1 - n_z^2\right)}\hat{\boldsymbol{z}} + \sqrt{\left(v_r + \Delta v_r\right)^2 \left(1 - n_r^2\right)}\hat{\boldsymbol{r}} + v_\theta \hat{\boldsymbol{\theta}}}{|\boldsymbol{v}_2| \sin(\theta)}, \tag{14}$$

where $n_z = \hat{\boldsymbol{n}} \cdot \hat{\boldsymbol{z}}$ and $n_r = \hat{\boldsymbol{n}} \cdot \hat{\boldsymbol{r}}$. The unit vector defining the transverse sputtering direction is then

$$\begin{aligned} \hat{\boldsymbol{t}} &= \hat{\boldsymbol{p}} \times \hat{\boldsymbol{n}}, \\ \hat{\boldsymbol{t}} &= -p_\theta n_r \hat{\boldsymbol{z}} + p_\theta n_z \hat{\boldsymbol{r}} + \left(p_z n_r - p_r n_z\right) \hat{\boldsymbol{\theta}}. \end{aligned} \tag{15}$$

Now, noting that $\hat{\boldsymbol{n}}$ points into the wall, we can define the velocity vector of an ejected boron atom as

$$\begin{aligned} \boldsymbol{v}_B &= -v_n \hat{\boldsymbol{n}} + v_p \hat{\boldsymbol{p}} + v_t \hat{\boldsymbol{t}}, \\ \boldsymbol{v}_B &= \left(-v_n n_z + v_p p_z - v_t p_\theta n_r\right) \hat{\boldsymbol{z}} \\ &\quad + \left(-v_n n_r + v_p p_r + p_\theta n_z\right) \hat{\boldsymbol{r}} \\ &\quad + \left(v_p p_\theta + v_t \left(p_z n_r - p_r n_z\right)\right) \hat{\boldsymbol{\theta}}. \end{aligned} \tag{16}$$

The velocity components v_n, v_p, and v_t are determined by sampling from velocity distribution functions (VDFs) calculated from the MD data. The forward and transverse velocity components, v_p and v_t, are sampled from Maxwell-Boltzmann distributions. Along the surface normal direction, a flux-biased Sigmund-Thompson distribution is used:[13,14]

$$f_{ST}(v_n) \propto \frac{v_n^3}{\left(v_n^2 + v_b^2\right)^{3 - 2m_{ST}}}. \tag{17}$$

The effective binding velocity is related to the surface binding energy as

$$E_b = \frac{1}{2} m_B v_b^2.$$

In general, the VDF parameters depend on the kinetic energy and incidence angle of the impacting ion. For ion energies greater than about 100 eV, the surface binding energy E_b from the Sigmund-Thompson distribution appears to become independent of ion energy and incidence angle and averages to about 4.5 eV.[6] The fit parameter m_{ST} is approximately zero for all MD simulation cases. The dependence of the Maxwellian mean velocity and temperature on ion energy and incidence angle has not yet been thoroughly investigated, so these values are fixed at values of $\bar{v}_p = \bar{v}_t = 0$ m/s and $T_p = T_t = 50,000$ K. The mean velocity components are consistent with the MD data for all ion energies at normal incidence. For oblique incidence angles, $\bar{v}_p$ can be as high as 3000 m/s. The forward and transverse temperature can be as low as 10,000 K or as high as 100,000 K depending on the ion energy and incidence angle. The value of 50,000 K chosen here falls between these extremes and is roughly consistent with 100 eV ions at normal incidence. The two VDFs used in the model—the Maxwellian VDF for the forward and transverse sputtering directions and the Sigmund-Thompson VDF for the surface normal direction—are shown in Fig. 2.

Once boron atoms are introduced at the channel walls, they are allowed to stream freely through the simulation domain. The effects of scattering collisions are neglected, so each macroparticle moves in a straight line from its point of origin until it exits the domain or strikes a surface. Any boron particles that strike a surface are assumed to condense and are thus removed from the system. As the boron atoms stream through the bulk plasma, it is possible for them to undergo electron impact ionization or excitation. A previous effort by Dragnea et al. using a direct simulation Monte Carlo (DSMC) technique showed a large disparity between the simulation results and CRDS measurements in the SPT-70 Hall thruster.[15] Since CRDS can only detect neutral, ground-state boron, it was hypothesized that excitation and ionization of boron may account for the differences between the simulations and experiment. Thus, single ionization of boron and excitation of ground-state neutral boron to the ^{4}P metastable state are included in the present work. The collision cross-sections for ionization come from the calculations of Kim and Stone,[16] whereas the cross-sections for excitation come from the calculations of Ballance et al.[17] The ^{4}P state is chosen because of its long life compared to other excited states[18] and because the collision cross-sections for excitation from the ground state are quite large. Note that while both ionization and excitation of boron are included, only excited boron atoms are tracked in the simulations. Boron ions are assumed to rapidly accelerate out of the thruster once they are created due to their very light weight compared to xenon. Hence, boron ionization serves only as a sink-term for ground-state boron in these simulations.

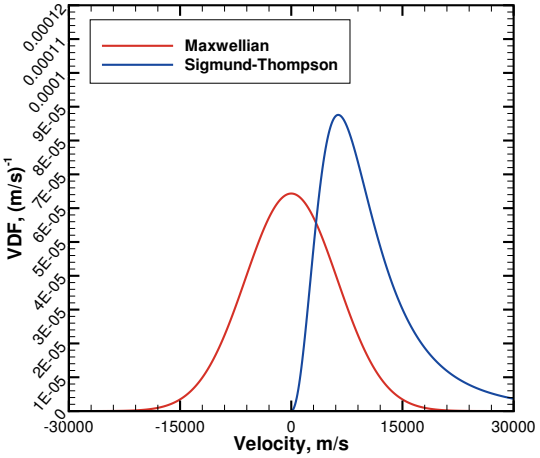

Figure 2: Maxwellian and Sigmund-Thompson VDFs of atomic boron used in the hybrid-PIC model.

D. Simulation setup

The thruster modeled in this work is NASA's 3.8 kW High-Voltage Hall Accelerator (HiVHAc).[19–22] The HiVHAc thruster development project is being conducted jointly by NASA Glenn Research Center (GRC) and Aerojet Rocketdyne. The present engineering development unit (EDU2) has demonstrated operation at discharge voltages of up to 650 V and discharge powers in excess of 4 kW. It is a highly throttleable device, with high-voltage modes achieving an I_{sp} approaching 2700 s and low-voltage modes achieving thrust-to-power ratios competitive with other state-of-the-art Hall thrusters.

Table 4: Discharge voltage and discharge current for the investigated operating points of HiVHAc.

Discharge voltage, V	Discharge current, A	
	Exp.	Sim.
500.5	1.99	2.00
500.1	3.94	4.02
500.6	6.04	6.08

The operating points investigated in this work are shown in Table 4. Both the measured and calculated discharge current are given. Testing of the thruster took place between Jan. 30th, 2015 and Feb. 2nd, 2015, in Vacuum Facility 12 (VF-12) at NASA GRC. No thrust were performed during the experiment. These operating points were also investigated by Lee et al. using CRDS.[23] CRDS measures the number density of the target species integrated along the laser path. To compare the 2D data produced by HPHall to the CRDS data, one must first integrate the boron density over the path of a virtual laser. Figure 3 shows a schematic of a virtual CRDS setup. The green line represents the laser, placed at a perpendicular distance

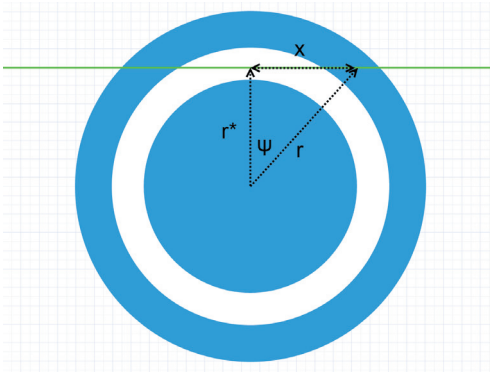

Figure 3: Schematic of a virtual CRDS setup, face-on view.

r^* from the thruster centerline. The coordinate x follows the path of the laser, so the path-integrated boron density is

$$n_{PI} = \int_{-\infty}^{+\infty} n_B\left(r\right) dx. \tag{18}$$

One can define x in terms of r^* and the angle ψ as

$$x = r^* \tan\left(\psi\right).$$

Similarly, the radial coordinate r can be defined as

$$r = \frac{r^*}{\cos\left(\psi\right)}.$$

Thus, Eq. 18 becomes

$$n_{PI}\left(r^*\right) = r^* \int_{-90^\circ}^{+90^\circ} \frac{n_B\left(\frac{r^*}{\cos(\psi)}\right)}{\cos^2\left(\psi\right)} d\psi. \tag{19}$$

In a real CRDS setup, the mirror cavity has a finite length. Lee reports a distance of 54 cm between mirrors,[23] so the integration limits of Eq. 18 become ± 27 cm, with corresponding angular bounds in Eq. 19. The integral is then evaluated numerically using a trapezoidal method to find the path-integrated boron density.

The HPHall simulation mesh consists of 70×30 cells. The base time step for each simulation is 5×10^{-8} s. The electron time step is $1/1250$ the base time step. Simulations are performed by first populating the domain with neutrals for 20,000 time steps. Then, the simulation is run with the plasma species turned on for 5000 time steps to allow startup transients to stabilize. The simulation is then run for 40,000 time steps to collect performance data. Once the agreement between the measured and calculated discharge current is satisfactory, 10,000 time steps are simulated with the boron submodel turned on, once for each of the Bohdansky parameter sets given in Table 2. The time-averaged 2D data from each of these simulations are saved and then processed using the steps outlined above.

III. Results and discussion

Figure 4 shows representative contours of plasma potential and electron temperature. These contours are provided in order to visualize the plasma flow-field and provide context for the following contours of boron density. Figure 5 shows calculated number density contours of ground-state boron and ^{4}P-state boron in HiVHAc operating at 500 V, 1 kW, for each of the Bohdansky fits presented in Table 2. The contours show that the peak density of the excited state is approximately three orders of magnitude smaller than that of the ground state for this operating point. For reference, the peak electron density is about a factor of 30 greater than the peak ground-state boron density computed using fit b. This suggests that electronic excitation does not significantly affect the density of ground-state boron in the thruster discharge channel and near-field plume. Comparing the simulation results, we see that Bohdansky fit b results in a greater boron density overall, as one would expect based on the value of γ.

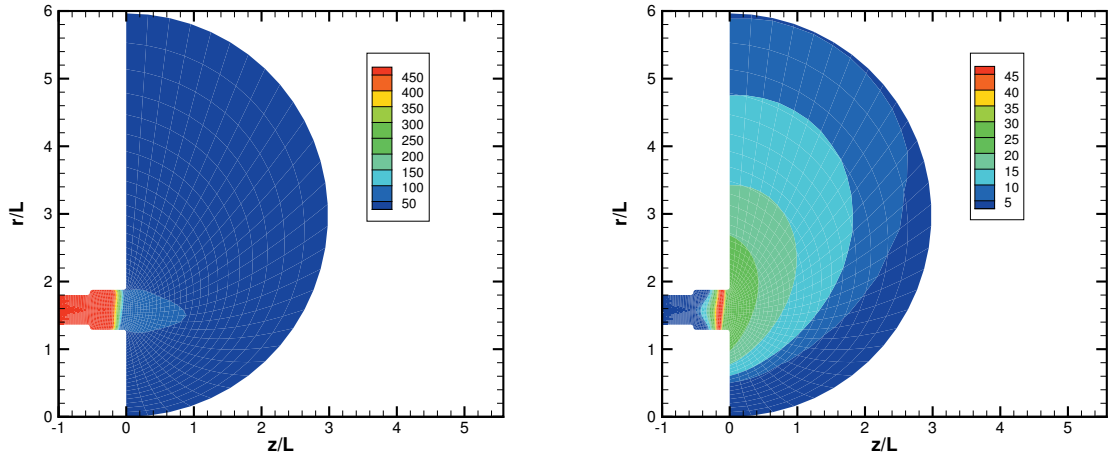

(a) Plasma potential, V **(b) Electron temperature, eV**

Figure 4: Computed contours of plasma potential and electron temperature in HiVHAc operating at 500 V, 2 kW. $z/L = 0$ **corresponds to the thruster exit plane.**

Figure 6 shows contours of boron excitation rate and ionization rate for 1 kW operation. Regardless of the Bohdansky fit used, the peak ionization rate is at least an order of magnitude greater than the peak excitation rate, indicating that ionization plays a much greater role than excitation in depleting the population of ground-state, neutral boron. However, the effects of ionization are still insignificant, as the reaction rate is too small to affect the ground-state boron density by more than a few percent.

Figure 7 shows the computed densities of ground- and ^{4}P-state boron for HiVHAc operating at 500 V, 3 kW. These results show the same trends as those at 1 kW: the density of the excited state is three orders of magnitude less than that of the ground state, and Bohdansky fit b results in a greater boron density overall compared to Bohdansky fit a. The peak density of ground-state boron is approximately a factor of 30 less than the electron density, as was the case for 1 kW operation. Compared to the 1 kW cases, the boron density is greater overall, as one would expect given the increase in discharge current. Thus, it appears that there is no unexpected change in behavior between the 1 kW and 3 kW operating points.

Figure 8 shows the path-integrated number density of ground-state boron as a function of the non-dimensional laser beam position P for each simulation case and for the CRDS measurements by Lee et al.[23] The non-dimensional beam position is defined as

$$P = \frac{r^* - r_{inner}}{r_{outer} - r_{inner}}.$$

The path-integrated boron density is computed 6 mm downstream of the thruster exit plane, consistent with Lee's experimental setup. The simulation results predict a more uniform distribution of boron overall, but otherwise they match the experimental measurements very well, especially when Bohdansky fit b is used. For $P \in (0, 1)$, the error relative to experiment does not exceed 60%. This implies that the amount of boron introduced into the simulation domain is physically realistic, and thus that the wall erosion rate is being estimated to reasonable accuracy. Given the numerous layers of assumptions between the MD sputtering model and HPHall, this level of agreement between the simulations and the experimental measurements is considered acceptable. Because the effects of boron excitation and ionization are shown to be negligible, one can also conclude that CRDS is an accurate tool for measuring the total density of boron in a Hall thruster plume. When corrected for boron atoms that do not escape the discharge channel, such measurements can be used to estimate the wall erosion rate *in situ*. Thus, these results show strong evidence that CRDS is a viable diagnostic for *in situ* measurement of Hall thruster channel erosion.

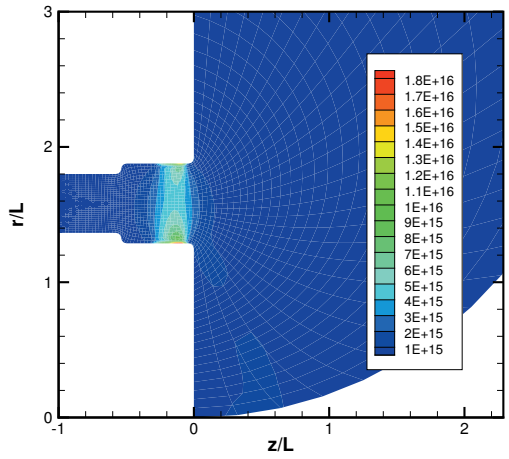

(a) Ground-state boron density, m^{-3}, fit a.

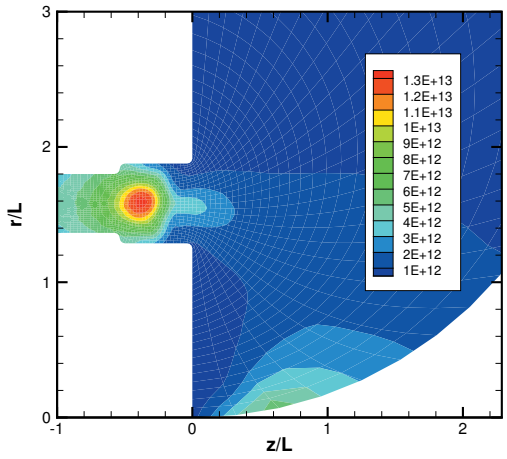

(b) ^{4}P-state boron density, m^{-3}, fit a.

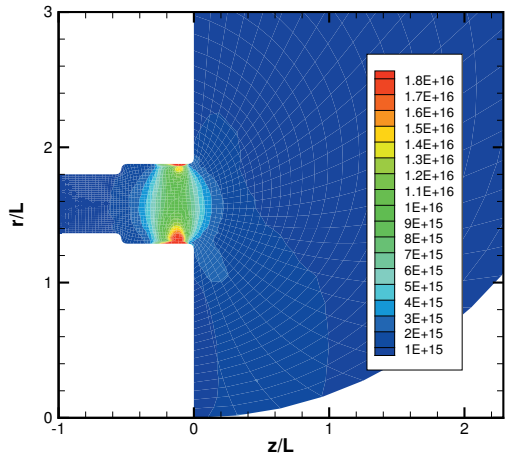

(c) Ground-state boron density, m^{-3}, fit b.

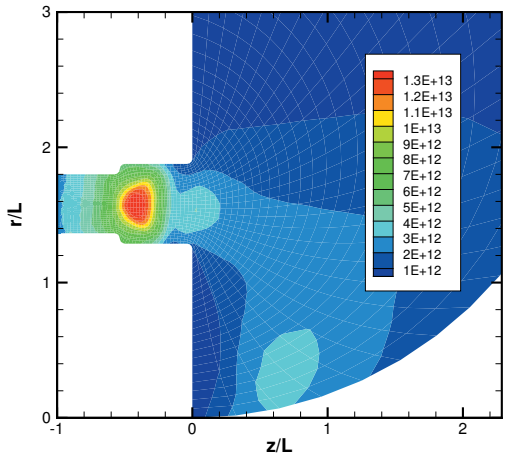

(d) ^{4}P-state boron density, m^{-3}, fit b.

Figure 5: Contours of boron density for HiVHAc operating at 500 V, 1 kW.

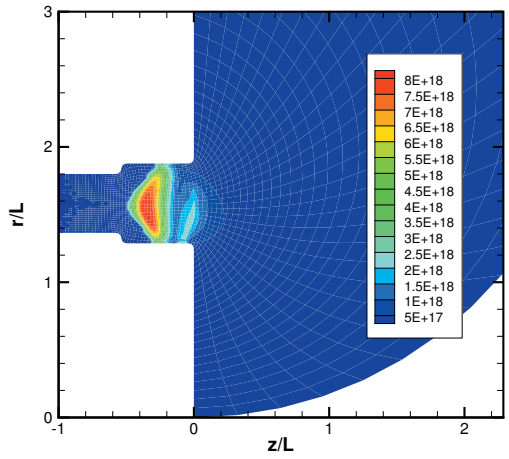

(a) Boron excitation rate, $m^{-3}s^{-1}$, fit a

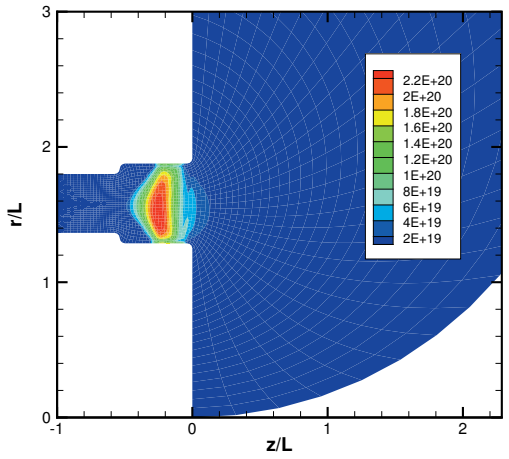

(b) Boron ionization rate, $m^{-3}s^{-1}$, fit a

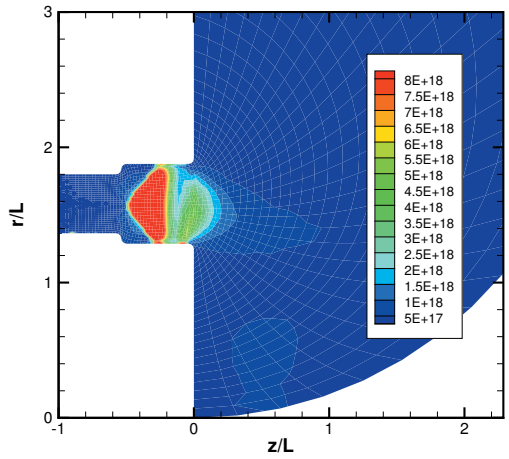

(c) Boron excitation rate, $m^{-3}s^{-1}$, fit b

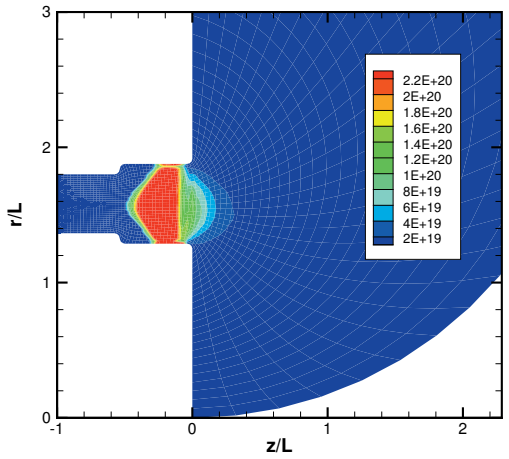

(d) Boron ionization rate, $m^{-3}s^{-1}$, fit b

Figure 6: Excitation and ionization rate of atomic boron in HiVHAc operating at 500 V, 1 kW.

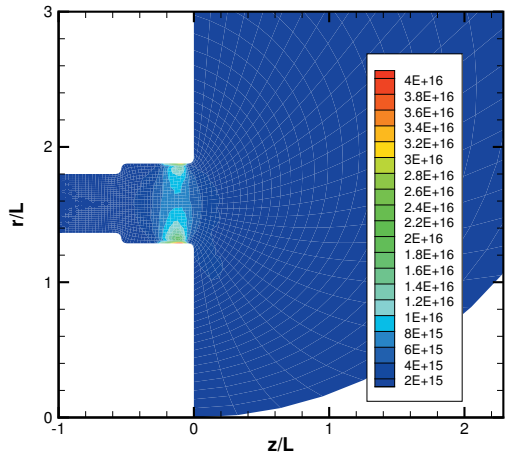

(a) Ground-state boron density, m^{-3}, fit a

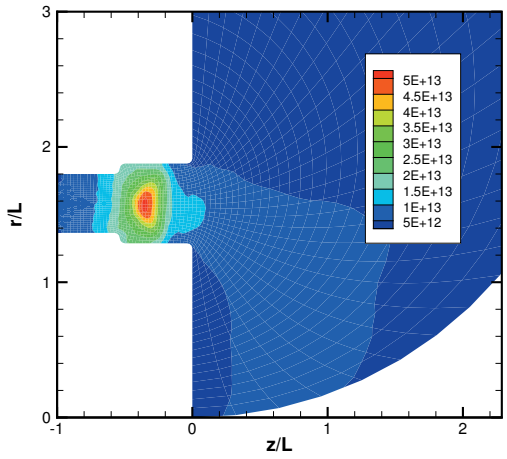

(b) ^{4}P-state boron density, m^{-3}, fit a

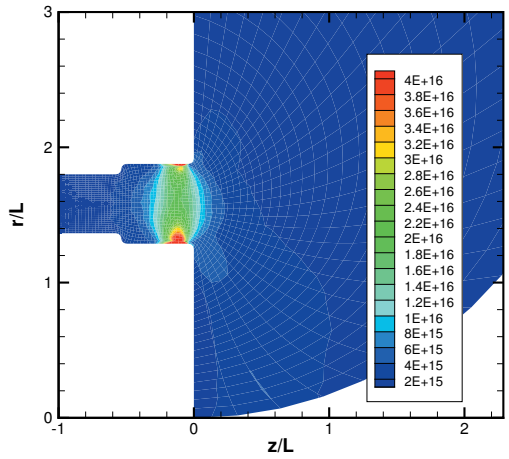

(c) Ground-state boron density, m^{-3}, fit b

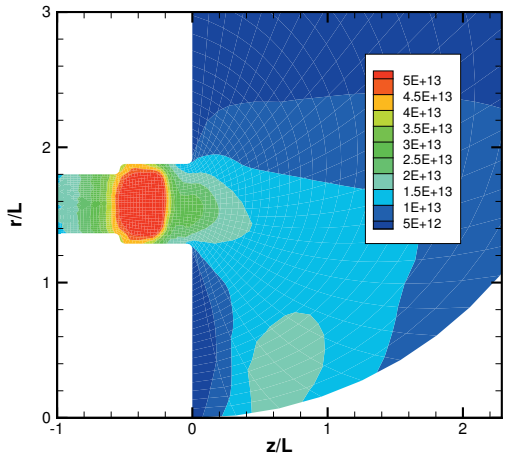

(d) ^{4}P-state boron density, m^{-3}, fit b

Figure 7: Contours of boron density for HiVHAc operating at 500 V, 3 kW.

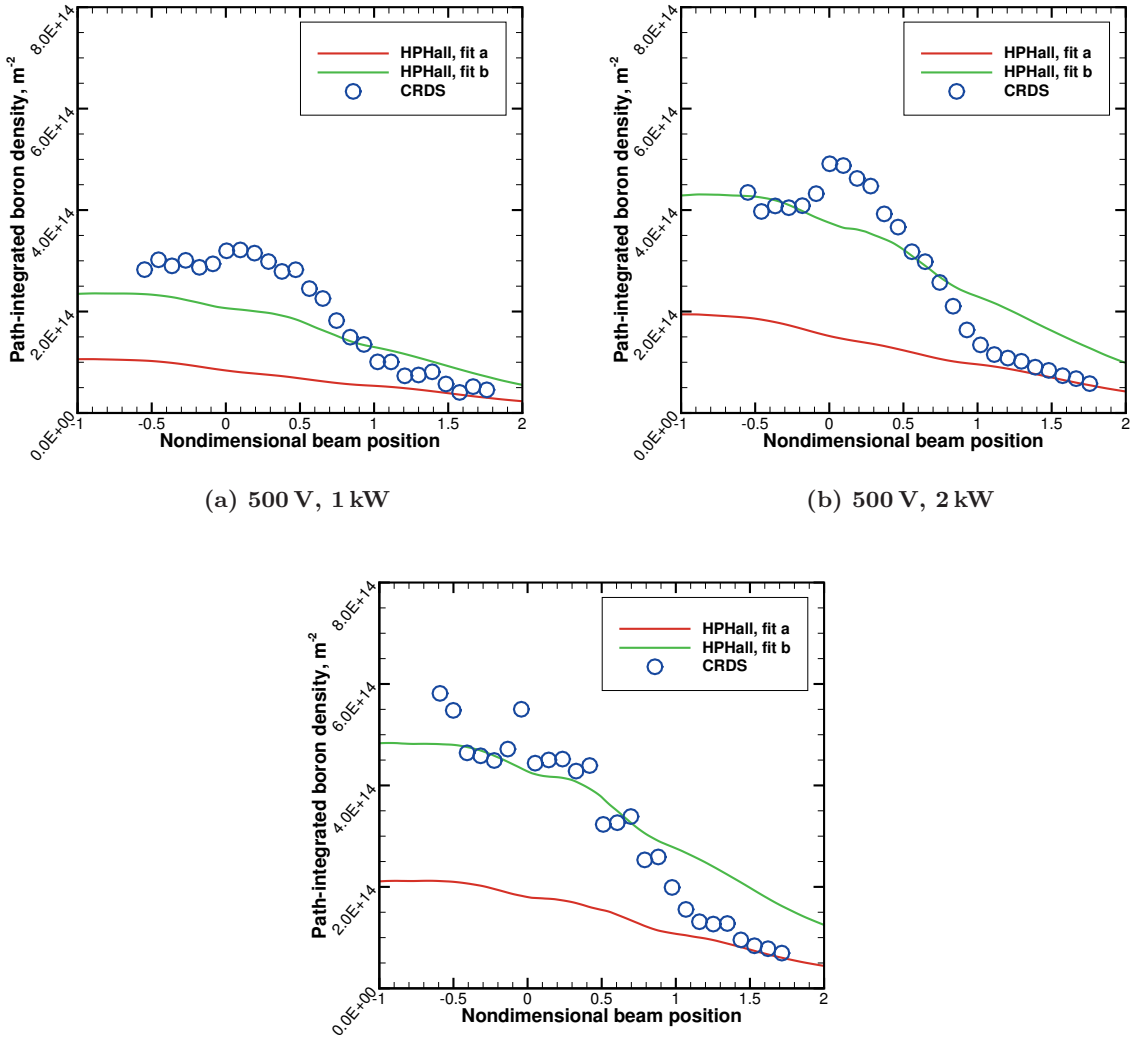

(a) 500 V, 1 kW

(b) 500 V, 2 kW

(c) 500 V, 3 kW

Figure 8: Path-integrated density of ground-state atomic boron as computed from the HPHall simulations and from the CRDS measurements.

IV. Conclusions and future work

In this work, the hybrid-PIC model HPHall was utilized to predict the transport of atomic boron through NASA's HiVHAc Hall thruster. The sputter yields of the *h*-BN walls and the 3D velocity distribution functions (VDFs) of the sputtered boron atoms were computed using a high-speed, physics-based molecular dynamics (MD) model. These data were then implemented within HPHall, and the resulting tool was used to simulate NASA's HiVHAc Hall thruster at a discharge voltage of 500 V and discharge powers of 1 kW, 2 kW, and 3 kW. The simulations showed that the peak number density of atomic boron is about 1.5 orders of magnitude less than the peak electron density for the operating conditions investigated. The density of the metastable ^{4}P state of boron was also calculated, and was shown to be approximately three orders of magnitude smaller than the density of ground-state boron. Comparing the rates of ionization and excitation of boron indicated that ionization has a greater impact on the density of ground-state, neutral boron, but is still negligible.

The computed density of ground-state, neutral boron was then compared to *in situ* measurements obtained by cavity ring-down spectroscopy (CRDS). For all operating points, the path-integrated boron density computed from the simulations agreed well with the experimental measurements. For laser positions between the inner and outer channel wall, the error between the simulations and the experiment did not exceed 60%. Because both excitation and ionization of boron have a negligible impact on the ground-state boron density, these results suggest that CRDS is an accurate tool for *in situ* measurement of the boron density in the thruster plume, and also provide evidence that CRDS is a viable erosion diagnostic.

The current model is capable of performing a numerical life test of the HiVHAc thruster. However, there were several assumptions made when implementing the sputter yield data into HPHall. Namely, the angular dependence of the sputter yield, as described by the Yamamura function, was assumed to be independent of the incident ion's energy. Also, the VDFs along the forward and transverse sputtering directions were assumed to be independent of ion energy and incidence angle. Including these dependencies is an obvious step towards improving the fidelity of the model. There is also some discrepancy between the BN temperature assumed in the sputter yield calculations and the typical temperature of the discharge channel walls in a Hall thruster. It is likely that including the temperature dependence of the sputter yields will influence the computed boron density. Finally, in order to fully validate CRDS as a tool for measuring erosion, the fraction of boron that redeposits on thruster surfaces must be quantified and its dependence on thruster operating point must be determined.

Acknowledgments

B. Smith would like to thank NASA for funding this research under a NASA Space Technology Research Fellowship, grant number NNX11AM64H. He would also like to thank Dr. Rohit Shastry of NASA GRC for providing the HiVHAc operating parameters used in the simulations.

References

[1]Gamero-Castaño, M. and Katz, I., "Estimation of Hall Thruster Erosion Using HPHall," IEPC Paper 2005-303, *29th International Electric Propulsion Conference*, Princeton, New Jersey, USA, Nov. 2005.

[2]Cheng, S., *Modeling of Hall thruster lifetime and erosion mechanisms*, Ph.D. thesis, Massachusetts Institute of Technology, 2007.

[3]Hofer, R. R., Mikellides, I. G., Katz, I., and Goebel, D. M., "BPT-4000 Hall thruster discharge chamber erosion model comparison with qualification life test data," IEPC Paper 2007-267, *30th International Electric Propulsion Conference*, Florence, Italy, 2007.

[4]Yim, J. T., *Computational Modeling of Hall Thruster Channel Wall Erosion*, Ph.D. thesis, University of Michigan, 2008.

[5]Yalin, A., Surla, V., Farnell, C., Butweiller, M., and Williams, J., "Sputtering studies of multi-component materials by weight loss and cavity ring-down spectroscopy," AIAA Paper 2006-4338, *42nd AIAA/ASME/SAE/ASEE Joint Propulsion Conference & Exhibit*, Sacramento, California, USA, July 2006.

[6]Smith, B. D. and Boyd, I. D., "Molecular Dynamics Computation of Steady-State Sputter Yields of Hexagonal Boron Nitride," IEPC Paper 2015-278, *34th International Electric Propulsion Conference*, Kobe, Hyogo, Japan, July 2015, to be published.

[7]Fife, J., *Hybrid-PIC Modeling and Electrostatic Probe Survey of Hall Thrusters*, Ph.D. thesis, Massachusetts Institute of Technology, 1999.

[8]Hofer, R., Katz, I., Mikellides, I., Goebel, D. M., Jameson, K. K., Sullivan, R. M., and Johnson, L. K., "Efficacy of

Electron Mobility Models in Hybrid-PIC Hall Thruster Simulations," AIAA Paper 2008-4924, *44th AIAA/ASME/SAE/ASEE Joint Propulsion Conference & Exhibit*, Hartford, Connecticut, USA, July 2008.

[9]Bohdansky, J., "A universal relation for the sputtering yield of monatomic solids at normal ion incidence," *Nuclear Instruments and Methods in Physics Research B*, Vol. 2, No. 1-3, 1984, pp. 587–591.

[10]Rubin, B., Topper, J., and Yalin, A., "Total and differential sputter yields of boron nitride measured by quartz crystal microbalance," *Journal of Physics D: Applied Physics*, Vol. 42, Oct. 2009, pp. 205205.

[11]Smith, B. D. and Boyd, I. D., "Computation of Total and Differential Sputter Yields of Boron Nitride Using Molecular Dynamics," IEPC Paper 2013-156, *33rd International Electric Propulsion Conference*, Washington, DC, USA, Oct. 2013.

[12]Yamamura, Y. and Shindo, S., "An empirical formula for angular dependence of sputtering yields," *Radiation Effects*, Vol. 80, No. 1-2, 1984, pp. 57–72.

[13]Sigmund, P., *Sputtering by Particle Bombardment I*, Vol. 47 of *Topics in Applied Physics*, chap. 2, Springer-Verlag, New York, 1981.

[14]Betz, G. and Wien, K., "Energy and angular distributions of sputtered particles," *International Journal of Mass Spectrometry and Ion Processes*, Vol. 140, No. 1, 1994, pp. 1–110.

[15]Dragnea, H. C., Boyd, I. D., Lee, B. C., and Yalin, A. P., "Characterization of Eroded Boron Atoms in the Plume of a Hall Thruster," IEPC Paper 2013-158, *33rd International Electric Propulsion Conference*, Washington, DC, USA, Oct. 2013.

[16]Kim, Y.-K. and Stone, P. M., "Ionization of boron, aluminum, gallium, and indium by electron impact," *Physical Review A*, Vol. 64, No. 5, Oct. 2001, pp. 052707.

[17]Ballance, C. P., Griffin, D. C., Berrington, K. A., and Badnell, N. R., "Electron-impact excitation of neutral boron using the R -matrix with the pseudostates method," *Journal of Physics B: Atomic, Molecular and Optical Physics*, Vol. 40, No. 6, March 2007, pp. 1131–1139.

[18]Fuhr, J. R. and Wiese, W. L., "Tables of Atomic Transition Probabilities for Beryllium and Boron," *Journal of Physical and Chemical Reference Data*, Vol. 39, No. 1, 2010, pp. 013101.

[19]Kamhawi, H., Manzella, D., Pinero, L., Haag, T., Mathers, A., and Liles, H., "In-Space Propulsion High Voltage Hall Accelerator Development Project Overview," AIAA Paper 2009-5282, *45th AIAA/ASME/SAE/ASEE Joint Propulsion Conference & Exhibit*, Denver, Colorado, USA, Aug. 2009.

[20]Kamhawi, H., Manzella, D., Pinero, L., Haag, T., and Huang, W., "In-Space Propulsion High Voltage Hall Accelerator Development Project Overview," AIAA Paper 2010-6860, *46th AIAA/ASME/SAE/ASEE Joint Propulsion Conference & Exhibit*, Nashville, Tennessee, USA, July 2010.

[21]Kamhawi, H., Haag, T., Pinero, L., Huang, W., Peterson, T., Manzella, D., Dankanich, J., Mathers, A., and Hobson, D., "Overview of the Development of a Low-Cost High Voltage Hall Accelerator Propulsion System for NASA Science Missions," AIAA Paper 2011-5520, *47th AIAA/ASME/SAE/ASEE Joint Propulsion Conference & Exhibit*, San Diego, California, USA, Aug. 2011.

[22]Kamhawi, H., Pinero, L., Haag, T., Peterson, T., Huang, W., Dankanich, J., Shastry, R., and Mathers, A., "High Voltage Hall Accelerator Propulsion System Development for NASA Science Missions," IEEE Paper 1095-323X, *2013 IEEE Aerospace Conference*, Big Sky, Montana, USA, March 2013.

[23]Lee, B. C., Yalin, A. P., Gallimore, A., Huang, W., and Kamhawi, H., "Real-Time Boron Nitride Erosion Measurements of the HiVHAc Thruster via Cavity Ring-Down Spectroscopy," IEPC Paper 2013-119, *33rd International Electric Propulsion Conference*, Washington, DC, USA, Oct. 2013.